# Dissociative recombination studies of $Ar_2^+$ by time-of-flight spectroscopy

G. B. Ramos, M. Schlamkowitz, J. Sheldon, and K. Hardy
*Florida International University, Miami, Florida 33199*

J. R. Peterson
*SRI International, Menlo Park, California 94025*
(Received 10 April 1995)

From time-of-flight spectra of metastable Ar* atoms emerging from sustained discharges in Ar, we observe discrete nonthermal peaks due to excited products of dissociative recombination (DR) of $Ar_2^+$ formed by reactions in the discharge. These peaks are in addition to the expected Boltzmann distributions of metastable atoms from direct excitation by fast primary electrons. From the peak velocities, and thus the kinetic energies released in the dissociation, the DR product states are uniquely determined, regardless of subsequent radiation. As we have previously found from $Kr_2^+$ [A. Barrios *et al.*, Phys. Rev. Lett. **69**, 1348 (1992)], most of the excited DR products are $(n+1)s$ states, but $Ar_2^+$ also yields smaller amounts of $4p$ and $3d$ states. We have also recently shown [G. B. Ramos *et al.*, Phys. Rev. A **51**, 2945 (1995)] that, surprisingly, in studies of $Ne_2^+$ and $Ar_2^+$ DR, a substantial but undetermined fraction of reactions go to a purely ground-state channel. In addition, we have found that under certain conditions in Ar discharges, the relative amount of the higher excited-state products, including $4p$, $3d$, $5s$, and $5p$ can be dramatically influenced. The velocity peaks also become narrower than expected from the thermal distribution of the parent $Ar_2^+$ as the energy level in the product atom increases. These studies in argon discharges have included variations in source pressure, discharge voltage, and strength of the axial magnetic field.

PACS number(s): 34.50.Lf

## I. INTRODUCTION

Because dissociative recombination (DR) is the only fast two-body process that can remove thermal free electrons and is thus the dominant electron-loss mechanism in low-temperature, low-pressure ionized molecular gases such as planetary ionospheres, laboratory electrical discharges [1], and interstellar clouds [2], it has been subject to numerous theoretical and experimental studies for about four decades. Most experiments have been confined to the measurement of reaction rates and only a few have managed to establish the product states, which are often very important in the chemistry of the medium. Two recent international conferences have been devoted to DR [3,4], which has also recently received renewed attention with the addition of storage-ring techniques to the experimental methods.

The final electronic states of the product atoms of the DR reaction in $Ne_2^+$, $Ar_2^+$, and $Kr_2^+$ were studied earlier by Mehr and Biondi [5] using optical spectroscopy on a pulsed discharge afterglow to identify the spectral lines emanating from the electronic states of the product atoms and thereby identify the product final electronic states. Recently in this laboratory, nonthermal metastable atoms effusing from sustained discharges in neon, argon, and krytpon gases have been studied using time-of-flight (TOF) spectroscopy [6–8]. The nonthermal distributions have been identified as products of DR reactions.

It has long been commonly believed that DR of free electrons with rare-gas dimer ions heavier than $He_2^+$, such as

$$e + Ar_2^+ \leftrightarrow (Ar_2^*)_{\text{unstable}} \rightarrow Ar^* + Ar + E_{Ke}, \qquad (1)$$

yields one atom in the $np^6$ ground-state configuration and the other predominantly in the $np^5(n+1)p$ excited state [9]. Here $E_{KE}$ indicates the dissociative kinetic energy (KE) released to the atoms. This belief arose because optical measurements [5] showed that the $(n+1)p$ radiation to the lower $(n=1)s$ states dominated over radiation from higher states and it was thought [10] that the repulsive potentials leading to the $(n+1)s$ excited products passed inside the inner turning point of the ground state of the ionic ion potential curve rather than intercept it, as required for a direct dissociative recombination process [11]. However, no radiation from the $(n+1)s$ product states could be observed because these states are either metastable or radiate in the vacuum ultraviolet, which was not detected in those experiments. TOF spectroscopy overcomes these difficulties as this technique allows direct observation of the KE released in the reaction. We have found convincing evidence that in fact $(n+1)s$ states dominate the excited DR products of all three species $Ne_2^+$, $Ar_2^+$, and $Kr_2^+$ [6–8]. We note that in a recent study by Malinovsky *et al.* [12], reporting DR production of $3p$ and $3d$ states from $Ne_2^+$ using a traditional optical technique, the authors displayed calculated potential-energy curves for $Ne_2^+$ and $Ne_2^*$ that indicated a curve crossing by $3s$ repulsive states near the inner turning point of the $Ne_2^+$ ground vibrational state, which provides a mechanism for our observed $3s$ production. A similar situation must occur in $Ar_2^+$ and $Kr_2^+$ even though, to our knowledge, it has not been shown. We report here the results of our study of the dissociative recombination of $Ar_2^+$ by time-of-flight spectroscopy. We have recently reported our observations of purely ground-state products of DR in $Ar_2^+$ [8] and here we focus on the higher-energy product states that we have observed.

The TOF technique used here has been previously described [6–8]. It allows the direct measurement of the KE

 

released in reaction (1). from $E_{KE}$ and the known values of the molecular ion internal energies, and assuming that the initial kinetic energy is thermal (near 0 eV) as expected [5], one can deduce the values of the electronic energies of the final atomic states. This determination is thus independent of any radiation subsequent to the dissociation.

## II. APPARATUS

The molecular-beam apparatus used here is the same as the one used previously [8]. The DR reaction occurs in a continuous discharge effusive source maintained by electrons produced by a directly heated thoria-coated tungsten ribbon ($2.5\times0.025$ mm$^2$). The source is surrounded by a solenoid that produces a variable axial magnetic field of up to 225 G. The gas pressure, the discharge current, the discharge voltage, and the applied magnetic field were variable in this work. We have previously discussed in detail the operation of this source with the applied magnetic field [13]. Within the discharge, the high-energy electrons (energies approximately equal to the discharge voltage in eV) create both excited states of atoms and atomic ions. Excited states are also produced by energetic secondary electrons following the ionizing collisions. At the pressures used here, molecular ions are formed principally by associative ionization

$$\mathrm{Ar}^* + \mathrm{Ar} \rightarrow \mathrm{Ar}_2^+ + e, \tag{2}$$

where Ar* is in a sufficiently high Rydberg state ($n>5$), or (2) could occur if both atoms are metastable. Subsequently, slow electrons undergo dissociative recombination with molecular ions to form fast neutral products. The effect of the axial magnetic field is to constrain the discharge, by constricting both fast and slow electrons to a narrow region along the axis, in alignment with the filament and the exit slit of the discharge. Thus excitation, ionization, and DR all occur close to the axis, which increases the observed yield of metastable atoms very effectively (by a factor of 10–100). Sweep plates located downstream from the source maintain an electric field of about 50 V/cm, which removes all charged particles and long-lived Rydberg states from the atom beam. The detector consists of a tungsten catcher plate from which Auger electrons are collected and detected by a Channeltron electron multiplier. Our system is sensitive only to atoms in the metastable state. This is due to several factors. First, fast neutral atoms (with the exception of ground-state direct product atoms) lack sufficient energy to eject electrons from the catcher plate. Second, charged products and atoms in the Rydberg state are removed from the beam at the sweep plates. Third, the flight time ($>200$ $\mu$sec) is long enough for all other species to decay.

## III. TREATMENT OF THE EXPERIMENTAL DATA

Knowing the ionization energy of a rare-gas atom $E_i$, the dissociation energy of the molecular ion $D_0$, and the energy of the final state $E_{FS}$, the dissociative kinetic energy $E_{KE}$ can be calculated using

$$E_{KE} = E_i - D_0 - E_{FS}. \tag{3}$$

Since we are dealing with homonuclear systems, the energy of the individual atoms $E_d$ is equal to one-half of $E_{KE}$. The ionization energy $E_i$ for argon is 15.76 eV [14]. The binding energy of the molecular ion $D_0$ is less well known. We used $1.23\pm0.03$ eV [15–17] for argon in our calculations. The energies and corresponding velocities for the states in the final product atom that are accessible in our experiment are shown in Table I.

We have shown [8] that the velocity of a DR product in the laboratory system is the sum of the c.m. thermal velocity, as given by a velocity distribution that is assumed to be Maxwellian and with a most probable velocity $v_p$, and the randomly directed velocity $v_{DR}$ of the DR reaction product in the c.m. system [8]. Thus the peak due to DR to a single final state is broadened by the Boltzmann distribution of the ions. The DR atom flux $dJ$ is then given in time space as [8]

$$dJ(t) = (c/t^4)\exp(-\{[(L/t) - v_{DR}]/v_p\}^2)dt. \tag{4}$$

In Eq. (4), $c$ is an arbitrary constant related to the flux of atoms from a particular transition, $L$ is the length of the flight path, and $t$ is the time of flight. The velocities expected $v_{DR}$ can be found from $E_{KE}$ in Eq. (3) for the DR reaction to a specific state in the product atom. DR occurs primarily with low-energy electrons [5], so the electron energy is assumed to be near zero. Under these conditions and the assumption that the $Ar_2^+$ parent is in its ground electronic and vibrational state, $v_{DR}$ is given in Table I. Our experimental data were fitted to the function in Eq. (4), where the free parameters were $c$, $v_p$, a function describing the background (either a constant or a straight line), and $t_0$, the time when the beam chopper opened. When more than one DR product was thought to be present in the experimental data to be fitted, Eq. (4) was summed over all the product velocities in the data. The fitting procedure used minimized $\chi^2$. When there was a question of which DR product was present in a particular time distribution, the time distribution was fitted with each possible DR product and the least-squares criterion (minimum $\chi^2$) was used to determine which product was dominant in the distribution. This procedure is subject to some uncertainty, but in most cases gave reasonable fits to the data.

## IV. DISCUSSION OF THE OBSERVED STATES

Figure 1 shows a time spectrum that we routinely observe from our discharge. It shows a small ground-state DR product peak, a much larger $4s$ DR product peak, and the Maxwellian velocity distribution of the thermal metastable atoms emanating from our discharge. This figure can be considered as a standard that can be compared to other spectra that we will discuss, which were taken with various source conditions.

The final product states that we have found to be present in our spectra under various conditions are shown in Table II. The corresponding velocities $V_{DR}$ and channel numbers can be found in Table I. Figure 2 shows a spectrum whose fit requires a total of six of these states. The states used in the fit are the $3p$ ground state (5907 m/sec, channel 5.2), the $4s$ and $4s'$ metastable states (2661 m/sec, channel 11.5), the $4p[1/2]$ $J=0$ state (1737 m/sec, channel 17.7), the

TABLE I. Calculated velocities and channel numbers for dissociative recombination in argon. The channel numbers shown are for our experimental apparatus where the flight path is 1.227 m and the time channel width is 40 $\mu$sec. The state designation is from Ref. [5].

| State designation | $J$ | Energy level ($cm^{-1}$) | (eV) | Velocity $v_{DR}$ (M/sec) | Channel number |
|---|---|---|---|---|---|
| $3p$ | 0 | 0 | 0 | 5906.883 | 5.19 |
| $4s[3/2]$ | 2 | 93 143.8 | 11.548 | 2675.795 | 11.46 |
| $4s[3/2]$ | 1 | 93 750.64 | 11.624 | 2641.819 | 11.61 |
| $4s'[1/2]$ | 0 | 94 553.71 | 11.723 | 2596.173 | 11.82 |
| $4s'[1/2]$ | 1 | 95 399.87 | 11.828 | 2547.192 | 12.04 |
| $4p[1/2]$ | 1 | 104 102.1 | 12.907 | 1974.155 | 15.54 |
| $4p[5/2]$ | 3 | 105 462.8 | 13.076 | 1868.738 | 16.41 |
| $4p[5/2]$ | 2 | 105 617.3 | 13.095 | 1856.39 | 16.52 |
| $4p[3/2]$ | 1 | 106 087.3 | 13.153 | 1818.311 | 16.87 |
| $4p[3/2]$ | 2 | 106 237.6 | 13.172 | 1805.965 | 16.99 |
| $4p[1/2]$ | 0 | 107 054.3 | 13.273 | 1737.339 | 17.66 |
| $4p'[3/2]$ | 1 | 107 131.8 | 13.283 | 1730.691 | 17.72 |
| $4p'[3/2]$ | 2 | 107 289.8 | 13.302 | 1717.048 | 17.86 |
| $4p'[1/2]$ | 1 | 107 496.5 | 13.328 | 1699.032 | 18.05 |
| $4p'[1/2]$ | 0 | 108 722.7 | 13.480 | 1587.966 | 19.32 |
| $3d[1/2]$ | 0 | 111 667.9 | 13.845 | 1282.487 | 23.92 |
| $3d[1/2]$ | 1 | 111 818.1 | 13.864 | 1264.929 | 24.25 |
| $3d[7/2]$ | 4 | 112 750.2 | 13.979 | 1150.012 | 26.67 |
| $3d[7/2]$ | 3 | 113 020.4 | 14.013 | 1114.491 | 27.52 |
| $3d[3/2]$ | 2 | 112 138.9 | 13.903 | 1226.585 | 25.01 |
| $3d[3/2]$ | 1 | 114 147.8 | 14.152 | 952.075 | 32.22 |
| $3d[5/2]$ | 2 | 113 426.1 | 14.063 | 1058.922 | 28.97 |
| $3d[5/2]$ | 3 | 113 716.6 | 14.099 | 1017.255 | 30.15 |
| $3d'[5/2]$ | 2 | 114 641.0 | 14.214 | 871.540 | 35.20 |
| $3d'[5/2]$ | 3 | 114 822.0 | 14.236 | 840.064 | 36.52 |
| $3d'[3/2]$ | 2 | 114 805.2 | 14.234 | 843.037 | 36.39 |
| $3d'[3/2]$ | 1 | 115 366.9 | 14.304 | 737.206 | 41.61 |
| $5s[3/2]$ | 2 | 113 468.6 | 14.068 | 1052.931 | 29.13 |
| $5s[3/2]$ | 1 | 113 643.3 | 14.090 | 1027.933 | 29.84 |
| $5s'[1/2]$ | 0 | 114 861.7 | 14.241 | 833.002 | 36.82 |
| $5s'[1/2]$ | 1 | 114 975.1 | 14.255 | 812.484 | 37.75 |
| $5p[1/2]$ | 1 | 116 660.1 | 14.464 | 398.079 | 77.06 |

$4p'[1/2]$ $J=0$ state (1588 m/sec, channel 19.3), the $3d[1/2]$ $J=0$ state (1282 m/sec, channel 23.9), and the $3d[7/2]$ $J=4$ state (1150 m/sec, channel 26.7). The data shown in Figs. 2(a) and 2(b) were taken with different discharge voltages; the other conditions were the same. The $4p'[1/2]$ $J=0$ and the $3d[7/2]$ $J=4$ states appear only in Fig. 2(a), while the $4p[1/2]$ $J=0$ state appears only in Fig. 2(b). The velocity used to fit the two metastable states, 2661 m/sec, is a weighted average of the velocities of the two states, weighted by their statistically expected amplitudes of 5/6 and 1/6. The source conditions used for these data were a pressure of 11 mTorr, a current of 220 mA, and a magnetic field of 175 G. The data of Fig. 2(a) were taken with a discharge voltage of 50 V, while the data of Fig. 2(b) were taken with a discharge voltage of 45 V.

The $3d'[3/2]$ $J=1$ (737 m/sec, channel 41.6) and the $5s'[1/2]$ $J=0$ (833 m/sec, channel 36.8) DR product states are illustrated in Fig. 3(a), superimposed on the thermal Maxwellian velocity distribution of the metastable atoms that are directly produced in the discharge. The velocity resolution of the apparatus is insufficient to completely resolve these two DR product states. Figure 3(a) also shows DR products to the $4s$ and $4s'$ metastable states. Figure 3(b) is an expanded plot of the TOF data in the range near the $3d'$ and $5s'$ DR direct products. The source conditions for these data were a pressure of 15 mTorr, a discharge voltage of 105 V, a discharge current 300 mA, and a magnetic field of 123.5 G.

Spectra that indicate DR reaction products in the $3d[5/2]$ $J=3$, $3d[3/2]$ $J=1$, $3d'[5/2]$ $J=2$, $5s'[1/2]$ $J=0$, $5s'[1/2]$ $J=1$, and $3d'[3/2]$ $J=1$ states are shown in Fig. 4. The fit to the data (line) in Fig. 4(a) requires DR to six final states of the product atoms whose velocities are near the most probable velocity of the thermal distribution. The figure also illustrates a laser deflection technique used to separate the two metastable states [8]. Briefly, a laser tuned to the 811.73-nm closed $4s[3/2]$ $J=2$ to $4p[5/2]$ $J=3$ transition is used to deflect atoms in the $4s$ $J=2$ metastable state from the atom beam. Figure 4(a) shows the laser-off time distribution, the laser-on time distribution, and a fit to the laser-on

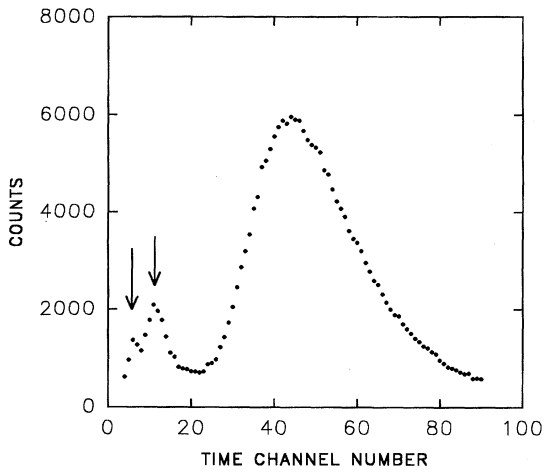


FIG. 1. Time distribution from our discharge showing the Maxwellian distribution of thermal atoms, DR products to the $4s$ states, and a small peak due to DR to the ground state. The arrows indicate the position of the ground-state product (left-hand arrow) and the $4s$ states (right-hand arrow).

time distribution. The data were best fit with the function in Eq. (4) corresponding to DR products in the $3d[3/2]$ $J=1$ (952 m/sec, channel 32.2) and the $5s'[1/2]$ $J=0$ (833 m/sec, channel 36.8) states. Figure 4(b) shows the difference between the laser-on and laser-off time spectra. Since only the $J=2$ metastable state is deflected, the difference is due only to atoms in the $J=2$ metastable state. The data were fit with four DR product functions [Eq. (4)] corresponding to the $3d[5/2]$ $J=3$ (1017 m/sec, channel 30.1), the $3d'[5/2]$ $J=2$ (871 m/sec, channel 35.2), the $3d'[3/2]$ $J=1$ (737 m/sec, channel 41.6), and the $5s'[1/2]$ $J=1$ (812 m/sec, channel 37.7) states. These states can all radiate to yield the $4p[3/2]$ $J=2$ state, which is deflected. The source conditions for these data were a pressure of 4 mTorr, a discharge voltage of 70 V, a discharge current 200 mA, and a magnetic field of 185 G.

DR to the $3d[5/2]$ $J=2$ (1058.9 m/sec, channel 29.0) state is shown in Fig. 5. This figure illustrates how, under some source conditions, the DR product can dominate the time spectrum. The source conditions were a pressure of 8 mTorr, a discharge voltage of 50 V, a discharge current of 290 mA, and a magnetic field of 134 G.

A spectrum showing DR reaction with products in the $5p[1/2]$ $J=1$ (398 m/sec, channel 77) state is shown in Fig. 6. This state is the highest-energy state (116 660.1 $cm^{-1}$, 14.464 eV) in the product atom accessible in our time-of-flight apparatus in its current configuration. The figure illustrates a time spectrum with DR to this state and a time spectrum without it. The two spectra were taken with different source conditions. The counting time on the later spectrum was selected so that the peak intensity of the Maxwellian time distribution was the same as the peak intensity of the former spectrum. The difference spectra and a fit to this difference using the function of Eq. (4) is shown in Fig. 6(b). These data were fit with a single DR function corresponding to DR to the $5p[1/2]$ $J=1$ state. The velocity was also a free parameter in this fit. The velocity determined from the fit was 363 m/sec, which is $35\pm5$ m/sec *slower* than the velocity calculated using the binding energy of $1.23\pm0.03$ eV for the $Ar_2^+$ molecule. If the energy of the electron causing the DR of the ionic molecule is assumed to be near zero, then we may calculate a binding energy of $1.245\pm0.007$ eV. The several determinations of the binding energy of $Ar_2^+$ are $1.23\pm0.02$ eV [15], $1.26\pm0.03$ eV [16], and $1.33\pm0.02$ eV [17]. Since the energy of the electron causing the DR in our apparatus is unknown and set to zero in our calculations, as is any internal energy in $Ar_2^+$, our value should be regarded as a lower limit on the binding energy of $Ar_2^+$. The small velocity width of the arrival time peak contributes to the uncertainty of 7 meV, which implies a narrow energy in the initial state.

TABLE II. Comparison of this work and the previous dissociative recombination work.

| Final-state designation | DR product $J$ | Energy level ($cm^{-1}$) | Present work | Biondi [13] (300 K) | Biondi [13] (7200 K) | Figure |
|---|---|---|---|---|---|---|
| $3p$ | 0 | 0 | yes | no | no | 2(a) |
| $4s[3/2]$ | 2 | 93 143.8 | yes | no | no | 2(a) |
| $4s'[1/2]$ | 0 | 94 553.71 | yes | no | no | 2(a) |
| $4p[1/2]$ | 0 | 107 054.3 | yes | yes | yes | 2(b) |
| $4p'[1/2]$ | 0 | 108 722.7 | yes | yes | yes | 2(a) |
| $3d[1/2]$ | 0 | 111 667.9 | yes | no | no | 2(a),2(b) |
| $3d[3/2]$ | 2 | 112 139 | yes | no | no | 10(d) |
| $3d[7/2]$ | 4 | 112 750.2 | yes | no | no | 2(a),5,7 |
| $3d[7/2]$ | 3 | 113 020.4 | yes | no | no | 10(c) |
| $3d[5/2]$ | 3 | 113 716.6 | yes | no | no | 4(b),7 |
| $3d[3/2]$ | 1 | 114 147.8 | yes | no | no | 4(a) |
| $3d'[5/2]$ | 2 | 114 641. | yes | no | no | 4(b) |
| $5s'[1/2]$ | 0 | 114 861.7 | yes | no | no | 3(a),3(b) |
| $5s'[1/2]$ | 1 | 114 975.1 | yes | no | no | 4(b) |
| $3d'[3/2]$ | 1 | 115 366.9 | yes | no | no | 3(a),4(b) |
| $5p[1/2]$ | 1 | 116 660.1 | yes | no | yes | 6 |

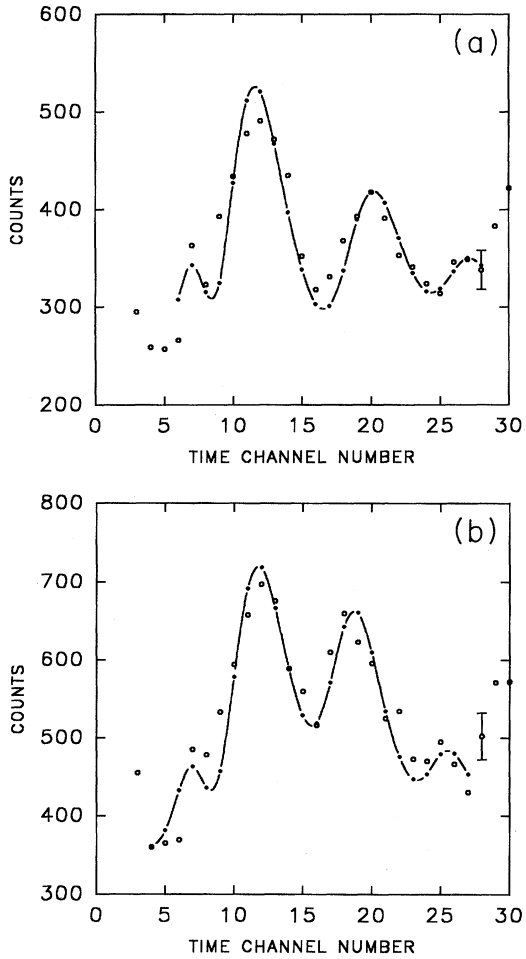


FIG. 2. Six direct product states of DR and a fit to the data. The data in (a) were fitted with functions [Eq. (3)] with velocities of 5907 m/sec (channel 5.2), 2661 m/sec (channel 11.5), 1588 m/sec (channel 19.3), 1282 m/sec (channel 23.9), and 1150 m/sec (channel 26.7). The data in (b) were fitted with DR functions with velocities of 5907 m/sec (channel 5.2), 2661 m/sec (channel 11.5), 1737 m/sec (channel 17.7), and 1282 m/sec (channel 23.9) (see the text).

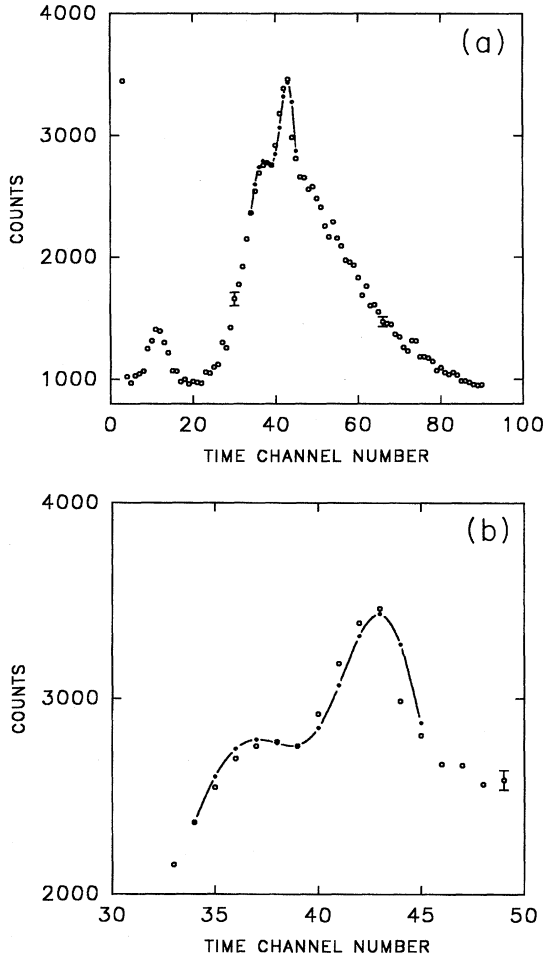


FIG. 3. DR to the $3d'[3/2]$ $J=1$ and the $5s'[1/2]$ $J=0$ states. The data in (a) show the Maxwellian distribution and DR to the metastable states. (b) is an expansion of the data in (a) around the DR peaks. The velocities of the peaks are 737 m/sec (channel 41.6) ($3d'$) and 833 m/sec (channel 36.8) ($5s'$).

DR to the $3d[7/2]$ $J=4$ and the $3d[5/2]$ $J=3$ states is shown in Fig. 7. Figure 7(a) shows the data and a fit to the DR peaks. These states were also shown in Figs. 2(a) and 4(b); however, the yield is markedly different. Figure 7(b) is an expanded plot that shows how well the theoretical function fits the data. The figure again illustrates how, under some source conditions, the products of the DR reaction completely dominate the thermal Maxwellian time distribution. These data and the fits illustrate similar data used to study the yields of these two states as a function of discharge parameters.

## V. YIELDS OF SOME OF THE FINAL PRODUCT STATES AS A FUNCTION OF DISCHARGE PARAMETERS

When the source is operated with no magnetic field, the $4s$ and $4s'$ DR products are the only ones readily observable. With various discharge conditions and with the applied magnetic field, the other DR products in Table II can be observed. We studied the yield of specific DR products under various discharge parameters, rather than the relative yield of one DR product to another, because we are unsure of the relative efficiency of our detection system as a function of the kinetic energy of the various DR products [8]. Since all charged particles and Rydberg states are removed from the atom beam by the sweep plates, the atom beam will contain only neutral particles. The shortest flight time we observe (that of the ground-state products) is 208 $\mu$sec, which gives all states except the two metastable states time to undergo radiative decay. This implies that, with the possible exception of the ground-state products, all the DR products we observe are in the metastable states. The direct ground-state products of DR do have sufficient kinetic energy to overcome the work function of our tungsten catcher plate, but the detection of ground-state atoms of these energies (5.5 eV) by a detector similar to ours is unknown (probably small). However, we have shown [8] that a substantial fraction of the ground-state DR products are reexcited in the discharge to

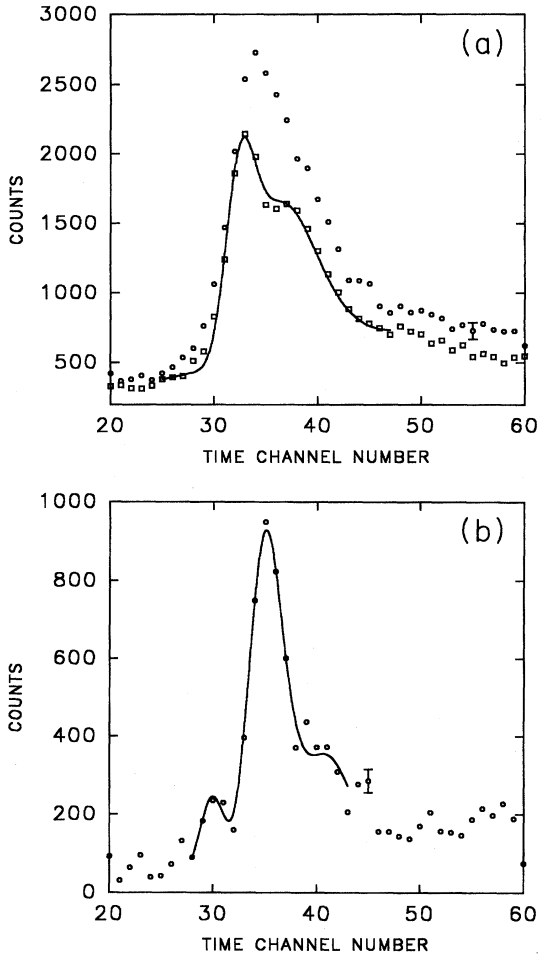


FIG. 4. DR direct products to the $3d[5/2]$ $J=3$, $3d[3/2]$ $J=1$, $3d'[5/2]$ $J=2$, $5s'[1/2]$ $J=0$, $5s'[1/2]$ $J=1$, and $3d'[3/2]$ $J=1$ states. In (a) the circles are laser off, the squares are laser on, and the line is a fit to the laser-on data. In (b) the circles are the difference data between laser on and off and the line is a fit to these data.

metastable states and are thus detected.

We have found that the yield of some DR product states varies sharply as a function of discharge parameters. The yields of the ground state, the $4s[3/2]$ $J=2$ and $4s'[1/2]$ $J=0$ metastable states, and the $3d[7/2]$ $J=4$, the $3d[5/2]$ $J=3$, the $3d[7/2]$ $J=3$, and the $3d[3/2]$ $J=2$ states have been studied as a function of discharge voltage, discharge pressure, and discharge magnetic field.

As will be seen, all of these parameters can influence the relative amount of various DR states, but the behavior is not easily understood. We found no significant variation in the production of any of these states as a function of discharge pressure in the range of pressures from 12 to 14 mTorr; however, at lower pressures of 1–4 mTorr we found significant variation in the production of the $3d$ states as a function of pressure. Figures 8(a) and 8(b) show the yield of the $4s$ and $4s'$ metastable states and ground-state direct products as a function of discharge voltage, with a discharge pressure of 12.5 mTorr and a magnetic field of 173 G. Figures 8(c) and

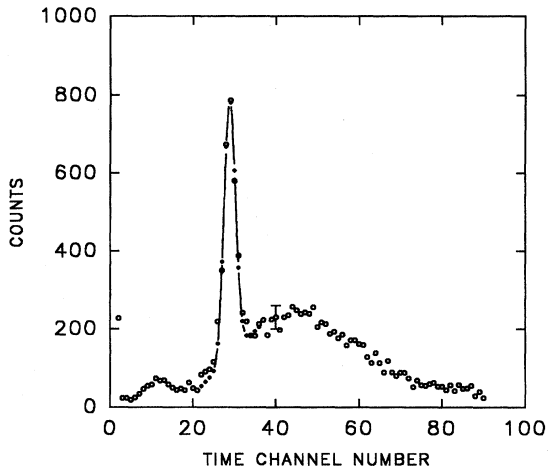


FIG. 5. Single DR direct product line to the $3d[5/2]$ $J=2$ state. Also shown is the Maxwellian velocity distribution and DR to the metastable states.

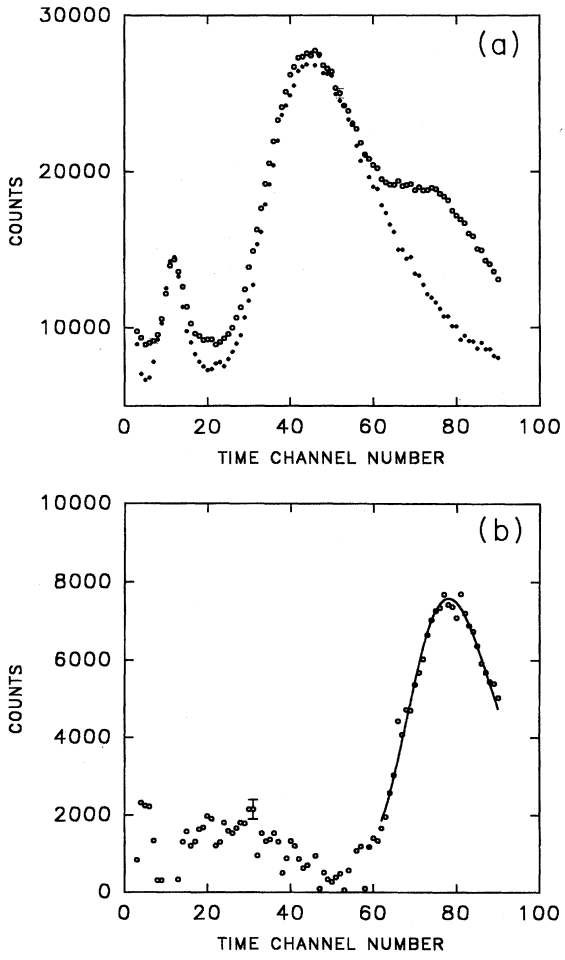


FIG. 6. DR to the $5p[1/2]$ $J=1$ state. (a) shows a time spectrum with DR (open circles) and one without DR. (b) is the difference between the two spectra in (a). The line is a fit to the data.

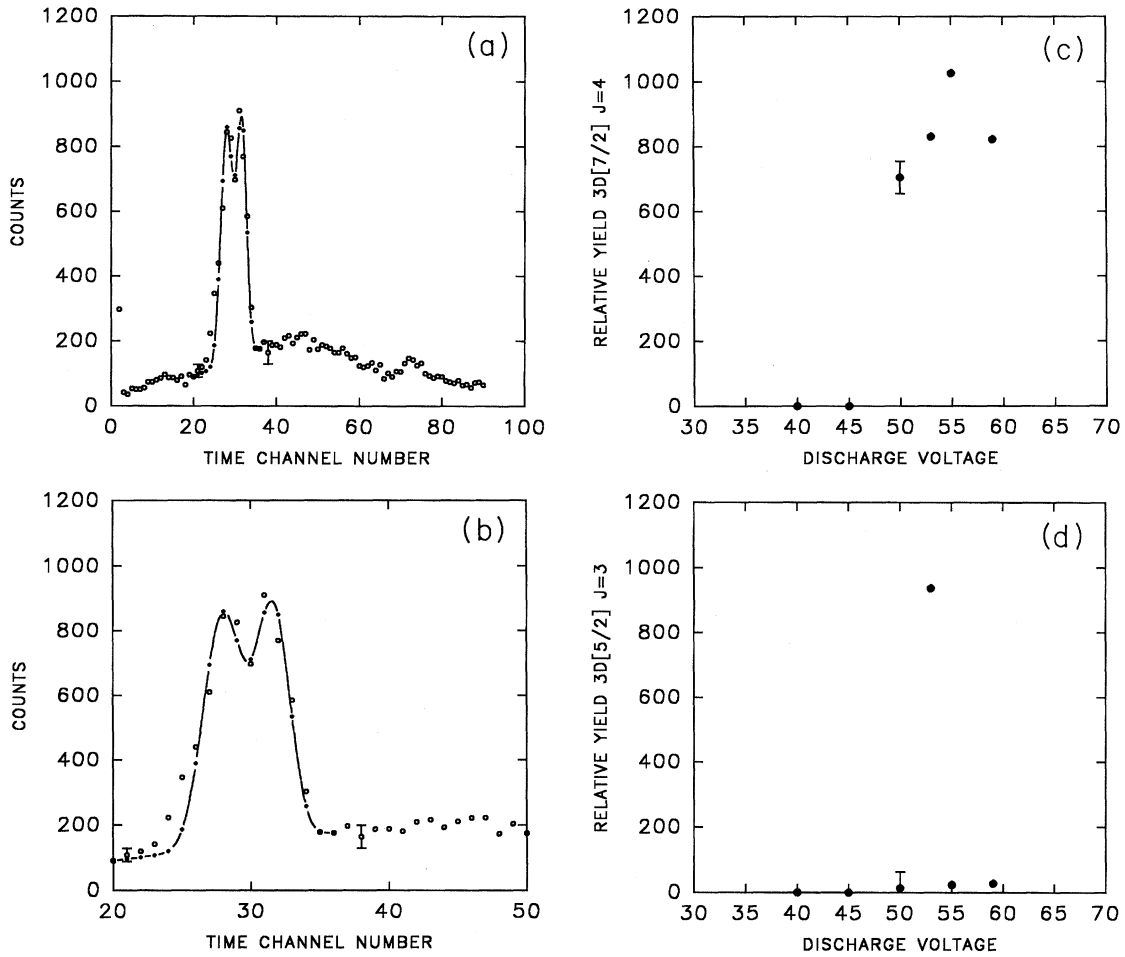


FIG. 7. Direct products of DR to the $3d[7/2]$ $J=4$ and $3d[5/2]$ $J=3$ states. The complete time spectrum is shown in (b) and an expansion of the spectra around the DR peaks is shown in (a). The yield of these two states as a function of discharge voltage is shown in (c) and (d).

8(d) show the yields of the combined $4s$ and $4s'$ metastable states and the ground state, respectively, as a function of magnetic field with a source pressure of 12.5 mTorr and a discharge voltage of 50 V. The vertical scales are all arbitrary. These data represent the DR product peak heights, after the subtraction of background.

Figures 7(c) and 7(d) show the relative yield of the $3d[7/2]$ $J=4$ and $3d[5/2]$ $J=3$ states as functions of discharge voltage. The data were determined by least-squares fitting to the function of Eq. (4) to the experimental data. The source pressure was 7 mTorr, the magnetic field was 144 G, and the discharge current was 290 mA.

We studied the yields of DR products in the $3d$ states at several discharge pressures in a range that allowed us to maintain all other discharge parameters at the same value. This study is illustrated in Figs. 9(a)–9(d). The discharge parameters used, other than pressure, were a magnetic field of 82 G, a discharge voltage of 50 V, and a discharge current of 200 mA. The pressure was varied from 1 to 4 mTorr. The data were all fitted using Eq. (4) in order to identify the states produced. We found that the most important $3d$ state observed varied with discharge pressure. Figure 9(a) illustrates the $3d[7/2]$ $J=4$ state, which was observed at a discharge pressure of 1 mTorr; Fig. 9(b) illustrates the $3d[5/2]$ $J=3$ state, observed at a pressure of 2 mTorr; Fig. 9(c) illustrates the $3d[7/2]$ $J=3$ state, observed at a pressure of 3 mTorr; and Fig. 9(d) shows the $3d[3/2]$ $J=2$ state, which was observed at a pressure of 4 mTorr.

## VI. WIDTHS OF THE OBSERVED DR PRODUCT PEAKS

As shown by Eq. (4), the width of the DR product velocity peaks contains information regarding the velocity distribution of the precursors of the DR reaction, presumed to be the $Ar_2^+$ molecule. Our data show a correlation between the fitted width of the DR peak and the dissociation energy. The width of the direct product lines and the associated final product states are shown in Table III. The correlation is shown in Fig. 10.

## VII. DISCUSSION

We have observed several final states in the DR of $Ar_2^+$ that have not previously been observed [5]. In the cases of

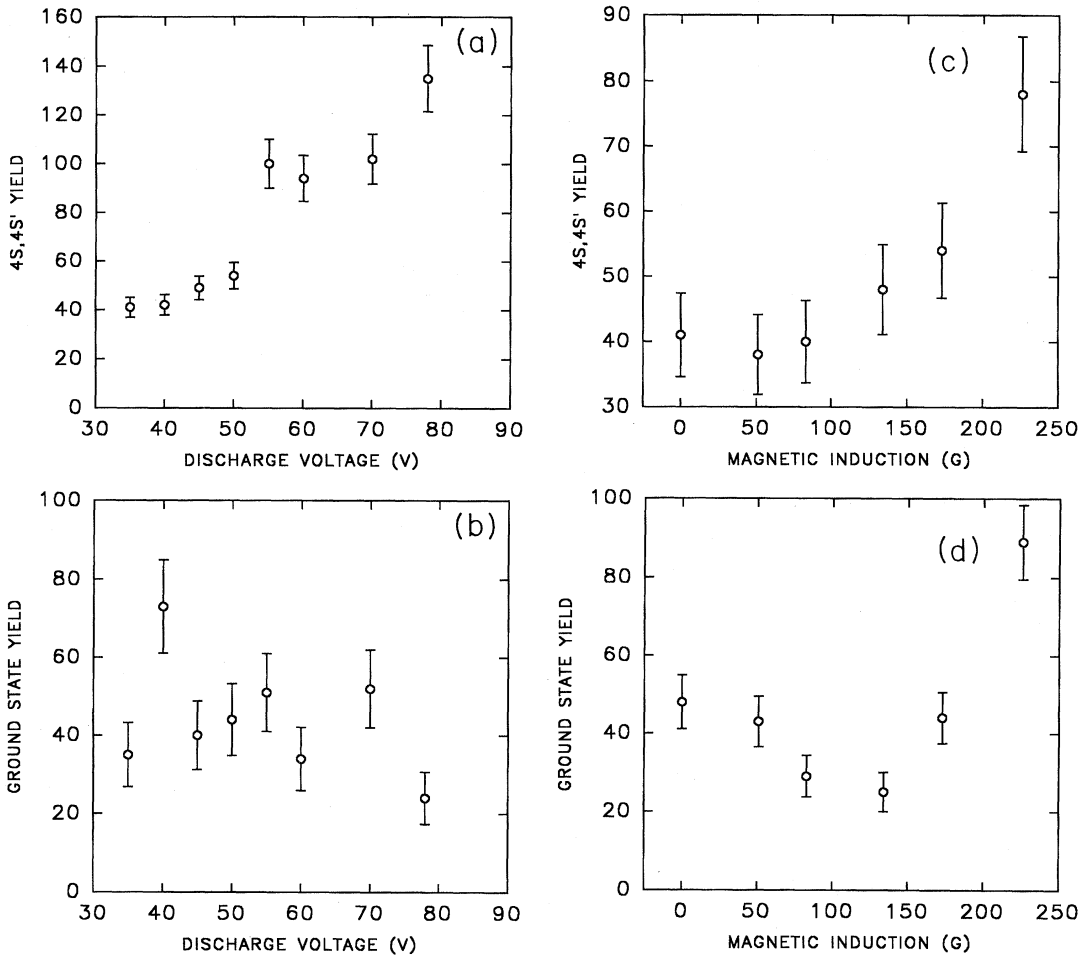


FIG. 8. Yield of the ground-state and the $4s$ and $4s'$ metastable-state DR products as a function of discharge parameters. The metastable-state DR products yield as a function of (a) discharge voltage and (c) magnetic field and the ground-state DR products yield as a function of (b) discharge voltage and (d) magnetic field.

the metastable states and the ground state, the previous experiments were not able to detect these states because they detected only the optical radiation from DR products in the discharge afterglow region. However, this is not the case in the case of the $4p$, $4p'$, $3d$, $3d'$, and $5s'$ states we observed as direct products of the DR reaction.

We can offer a qualitative explanation for the yields of some of the observed DR transitions. Previously, we studied the effects of the application of a longitudinal magnetic field to our glow discharge [13]. The $Ar_2^+$ is primarily formed through associative ionization by reactions such as (2), which depends on the formation of a high ($n>5$) Rydberg state Ar*, or it can be formed by two metastable atoms. Rydberg states would also decay along the flight path to the metastable states, so one would expect that the formation of the metastable states would follow the same trend as the formation of the Rydberg states in the discharge. One would also expect that the yield of DR products would also follow the trend of the data defining the production of $Ar_2^+$. Our data are consistent with these expectations. The trend of the $4s$ and $4s'$ final product yields versus applied magnetic field shown in Fig. 8(c) clearly follows the trend we have observed for the production of thermal metastable states in our discharge. The yield of ground-state atoms as shown in Fig. 8(d) also follows that same trend, though it is obvious that there are other mechanisms involved in the production and observation of the ground-state direct products that are not involved in $4s$ and $4s'$ production. Regarding our study of the DR yields as functions of discharge voltage, we note that Becker and Lampe [18] studied the production of the $Ar_2^+$ molecule as functions of electron energy using pulsed mass spectroscopy. The argon pressures they used, 5–8 mTorr, were slightly lower than our discharge pressures. We digitized the $Ar_2^+$ data shown in their paper for the shortest delay time they used and reproduce it in Fig. 10. Compared to our data in Fig. 8(b), Fig. 10 shows a similar increase in relative yield at approximately 35–40 V and a second broad feature, peaking at a lower yield, at approximately 70 V. Taken together, we conclude that our observed DR yields for the ground $4s$ and $4s'$ states increase with the production of both Ar* metastable states and $Ar_2^+$ molecules, as expected.

The production of $3d[5/2]$ $J=3$ and $3d[7/2]$ $J=4$ states was also studied as a function of discharge voltage as in Figs. 7(c) and 7(d). Since it is generally thought that a curve cross-

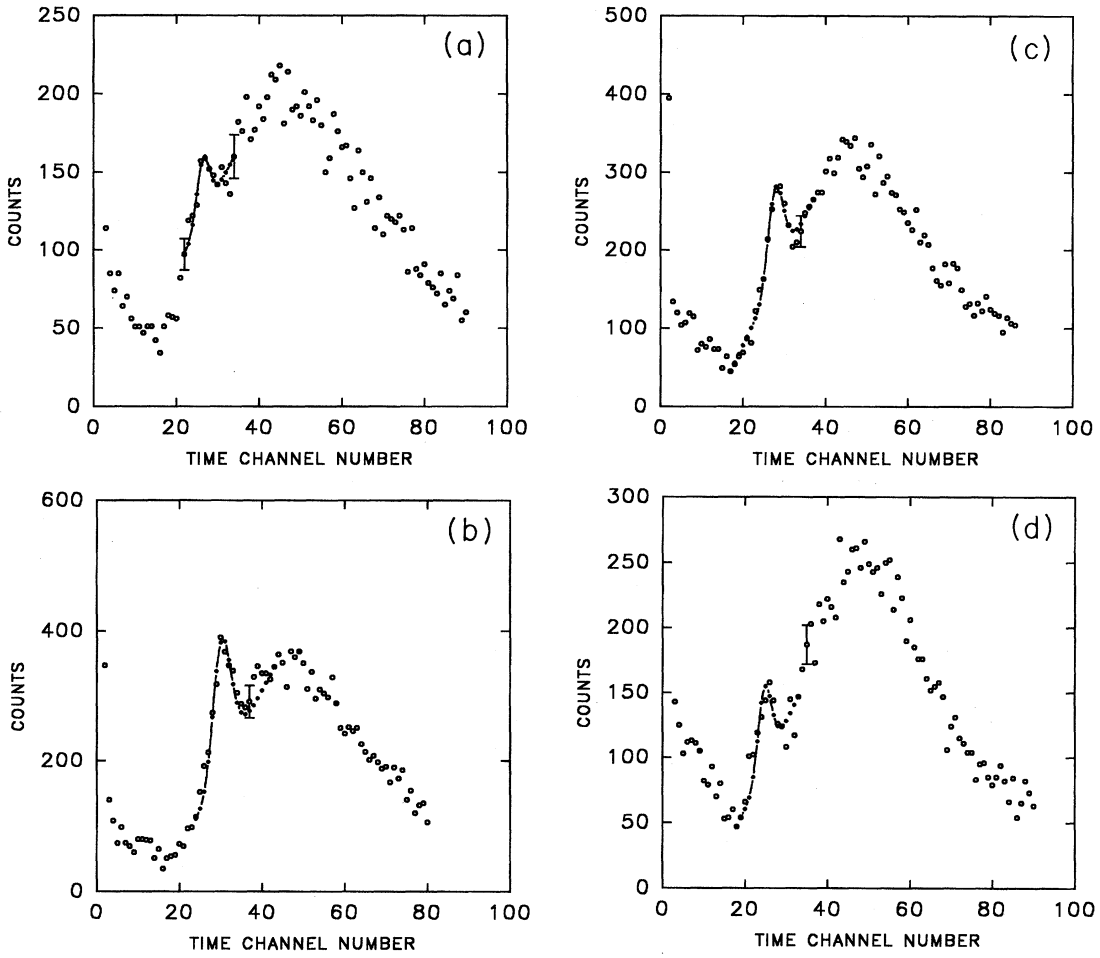


FIG. 9. Pressure dependence of the production of DR direct products to some $3d$ states. (a) The $3d[7/2]$ $J=4$ state is produced at a pressure of 1 mTorr, (b) the $3d[5/2]$ $J=3$ state is produced at 2 mTorr, (c) the $3d[7/2]$ $J=3$ state is produced at 3 mTorr, and (d) the $3d[3/2]$ $J=2$ state is produced at 4 mTorr.

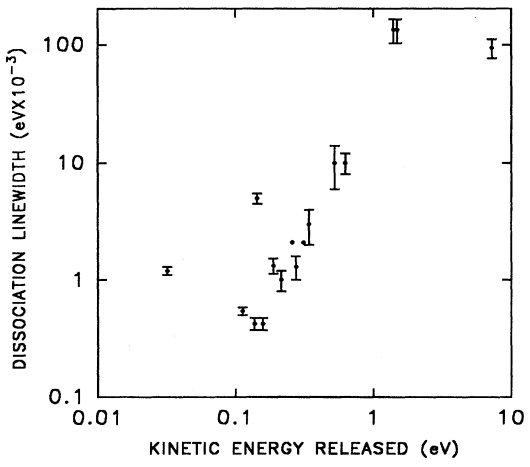


FIG. 10. Widths of the DR direct product lines as determined from the fitting of the data to the function Eq. (4). Note the grouping of the ground $4s$ and $4s'$ states at approximately 100 eV width.

ing is required in an efficient DR process, and clearly our data show that these final product states occur in a very narrow range of discharge voltages, a possible explanation would be that some electric fields in the discharge cause a coupling between the initial attractive ($Ar_2^+ + e^-$) transient Rydberg state and the repulsive states that dissociate to Ar($3d[5/2]$ $J=2$) or Ar($3d[7/2]$ $J=4$) and the ground-state argon atom. This is not a totally unreasonable assumption, since a strong perturbation, such as a pseudocurve crossing, is generally considered essential for efficient DR, and clearly our data show that these product states can be produced in our discharge. Such predissociations by small fields have been seen in high-$n$ states of $H_2$ by Helm (see Ref. [4], p. 145).

The observed widths of the direct product lines is also puzzling. As can be seen in Fig. 10, the widths fall into two groups, with the DR lines corresponding to the ground $4s$ and $4s'$ states being approximately the width expected if the parent molecules had velocity distributions approximately equal to the velocity distribution of the metastable atoms effusing from our source. States other than the ground and metastable states are considerably narrower. Clearly, these

TABLE III. Dissociation energies and width of dissociation lines.

| Final-state designation | DR product $J$ | Energy level ($cm^{-1}$) | Kinetic energy (eV) | Kinetic energy (m/sec) | Width ($10^{-3}$ eV) | Width (m/s) |
|---|---|---|---|---|---|---|
| $3p$ | 0 | 0 | 7.27 | 5907 | 94±17 | 675±125 |
| $4s[3/2]$ | 2 | 93 143.8 | 1.49 | 2673 | 133±30 | 800±200 |
| $4s'[1/2]$ | 0 | 94 553.71 | 1.40 | 2594 | 133±30 | 800±200 |
| $4p[1/2]$ | 0 | 107 54.3 | 0.628 | 1735 | 10±2 | 225±25 |
| $4p'[1/2]$ | 0 | 108 722.7 | 0.525 | 1586 | 10±4 | 225±90 |
| $3d[1/2]$ | 0 | 111 667.9 | 0.342 | 1281 | 3±1 | 122±70 |
| $3d[3/2]$ | 2 | 112 139. | 0.312 | 1226 | 2.1±0.1 | 100±20 |
| $3d[7/2]$ | 4 | 112 750.2 | 0.275 | 1148 | 1.3±0.3 | 80±40 |
| $3d[7/2]$ | 3 | 113 020.4 | 0258 | 1111 | 2.1±0.1 | 100±20 |
| $3d[5/2]$ | 3 | 113 716.6 | 0.215 | 1016 | 1.0±0.2 | 70±30 |
| $3d[3/2]$ | 1 | 114 147.8 | 0.188 | 950 | 1.33±0.2 | 80±10 |
| $3d'[5/2]$ | 2 | 114 641. | 0.158 | 869 | 0.42±0.05 | 45±5 |
| $5s'[1/2]$ | 0 | 114 861.7 | 0.144 | 831 | 5.0±0.5 | 155±15 |
| $5s'[1/2]$ | 1 | 114 975.1 | 0.137 | 811 | 0.42±0.05 | 45±5 |
| $3s'[3/2]$ | 1 | 115 366.9 | 0.13 | 737 | 0.54±0.04 | 51±6 |
| $5p[1/2]$ | 1 | 116 660.1 | 0.032 | 395 | 1.2±0.1 | 78±9 |

widths indicate that the precursors of the DR reactions that yield the ground and $4s$,$4s'$ states come from a group of atoms in reaction (2) that have a velocity distribution that is approximately Maxwellian, with a most probable velocity close to that of the metastable argon atoms in the discharge. These reactions could occur in the positive column of the discharge and the $Ar_2^+$ ions would then have approximately thermal velocity distributions. All DR reaction products that we have observed, whose velocity distributions were narrower than those expected from a thermal distribution of $Ar_2^+$ ions, are states that are only produced under specific discharge conditions; for example, see Figs. 7(c), and 7(d) as well as Fig. 9. If the $Ar_2^+$ ions have subthermal velocity distributions, as they clearly do, it may be related to the fact that these outgoing states are so near the ionization limit that the reaction can yield only separated DR product atoms in the subthermal range of velocities. These narrow velocity distributions resulting from direct products to higher-lying states in the product atom are clearly not understood. However, it should be noted that if DR yields these higher-lying states from $Ar_2^+$ ions with the normal Maxwellian velocity distribution characteristic of our discharge, they would not be observed because the velocity distribution on precursor $Ar_2^+$ ions would broaden the DR product TOF distribution until it was not observable.

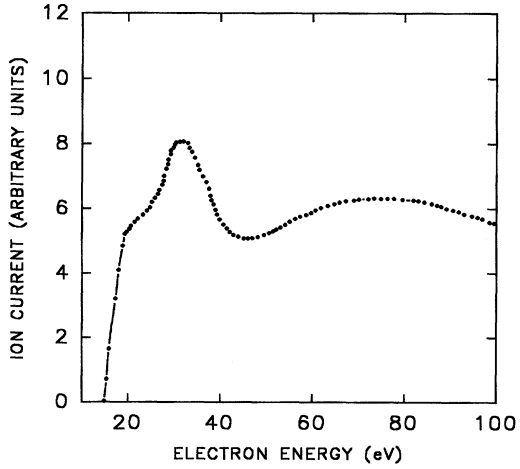


FIG. 11. Data of Becker and Lampe [18]. The data shown in their paper, most appropriate to our experimental situation, were digitized and plotted.

## VIII. SUMMARY

We have used a TOF technique to study the final product states of the DR reaction in $Ar_2^+$ by the observation of nonthermal distributions of metastable atoms emerging from a discharge. Under normal unperturbed conditions the dominant excited products of DR are the $4s$ and $4s'$ states, but an undetermined non-negligible fraction goes to purely ground states. None of these channels is explainable by current theoretical potential calculations, whose focus has been on the dimer states that radiate at larger internuclear distances that are not important in DR. When an axial magnetic field is applied, the density of dimer ions in the discharge increases greatly. Under these conditions, we observed substantial yields of $4p$, $3d$, $3d'$, $5s'$, and $5p$ states, with varying relative amounts that depend on discharge conditions. Certain conditions seem to emphasize certain product channels, indicating that the couplings to these states can be affected by local conditions. Our observations of the widths of the DR product TOF distributions reflect the velocity distributions on the parent $Ar_2^+$ ions plus any energy acquired from the recombining electrons. The narrow velocity widths of these higher state channels shows that there must be a supply of subthermal electrons in the source and also that the DR

events that contribute to these peaks must occur where the ions are also subthermal.

## IX. CONCLUSION

Clearly, much theoretical work must be done to explain some of our experimental results and it is hoped that this paper will stimulate interest and theoretical work on the DR reaction in $Ar_2^+$ under unperturbed conditions and also how the DR reaction can be affected by local and external electric and magnetic fields in argon discharges. We have shown that, although it can provide only qualitative information on product branching ratios, the time-of-flight method of studying these reactions is a valuable tool in providing detailed information for these theoretical investigations that cannot be obtained by optical observations. The TOF method used here is primarily effective for the rare-gas dimers, whose metastable states are not only observable because of their high energy but also because all higher Rydberg states can radiate to them during the flight time. The energy resolution available from the TOF method is much better than other methods when applied to the slower direct products and we know of no other method that can provide information on the velocity distributions of the precursors of the DR reaction.

## ACKNOWLEDGMENTS

G.B.R., M.S., J.S., and K.H. received partial support from AFOSR Grant No. F49620-93-1-0159DEF. J.S. received partial support from NASA Grant No. NAG 5-2583.

[1] W. G. Graham, in *Dissociative Recombination: Theory, Experiment and Applications* (Ref. [3]), p. 194.

[2] J. H. Black and E. V. van Dischoeck, in *Dissociative Recombination: Theory, Experiment, and Applications* (Ref. [3]), p. 317.

[3] *Dissociative Recombination: Theory, Experiment, and Applications*, edited by J. B. A. Mitchel and S. L. Guberman (World Scientific, Singapore, 1989).

[4] *Dissociative Recombination: Theory, Experiment, and Applications*, edited by B. R. Rowe, J. B. A. Mitchell, and A. Canosa (Plenum, New York, 1993).

[5] F. J. Mehr and M. A. Biondi, Phys. Rev. **176**, 322 (1968).

[6] K. A. Hardy, E. Gillman, and J. Sheldon, J. Appl. Phys. **67**, 7240 (1990).

[7] A. Barrios, J. W. Sheldon, K. A. Hardy, and J. R. Peterson, Phys. Rev. Lett. **69**, 1348 (1992).

[8] G. B. Ramos, M. Schlamkowitz, J. Sheldon, K. A. Hardy, and J. R. Peterson, Phys. Rev. A **51**, 2945 (1995).

[9] D. L. Heustis, in *Applied Atomic Collision Physics*, edited by E. W. McDaniel and W. L. Nighan (Academic, New York, 1982); M. A. Biondi, *ibid.*

[10] D. C. Lorents, Physica B+C **82C**, 19 (1976).

[11] J. N. Bardsley, J. Phys. B **1**, 365 (1968).

[12] L. Malinovsky, P. Lukáš, J. Trnovec, C. J. Hong, and A. Tálsky, Czech. J. Phys. **40**, 191 (1990).

[13] A. Barrios, G. B. Ramos, K. A. Hardy, and J. W. Sheldon, J. Appl. Phys. **76**, 728 (1994).

[14] C. E. Moore, *Atomic Energy Levels*, Natl. Bur. Stand. (U.S.) Circ. No. 467 (U.S. GPO, Washington, DC, 1949), Vol. I.

[15] P. M. Dehmer and S. T. Pratt, J. Chem. Phys. **76**, 843 (1982).

[16] C. Y. Ng, D. J. Trevor, B. H. Mahan, and Y. T. Lee, J. Chem. Phys. **66**, 446 (1977).

[17] J. T. Mosley, R. P. Saxon, B. A. Huber, P. C. Crosby, A. Abouaf, and M. Tadjeddine, J. Chem. Phys. **67**, 1659 (1977).

[18] P. M. Becker and F. W. Lampe, J. Chem. Phys. **42**, 3857 (1965).